

Article

# Nonlinear Robust Control of a New Reconfigurable Unmanned Aerial Vehicle

Saddam Hocine Derrouaoui \* , Yasser Bouzid and Mohamed Guiatni

Complex Systems Control & Simulators (CSCS) Laboratory, Ecole Militaire Polytechnique, Bordj el Bahri 16046, Algeria; yasseremp@gmail.com (Y.B.); mohamed.guiatni@gmail.com (M.G.)

\* Correspondence: derrouaouish@gmail.com

**Abstract:** In this paper, a nonlinear robust Fast Terminal Sliding Mode Controller (FTSMC) is designed to control and stabilize a new reconfigurable Unmanned Aerial Vehicle (UAV) in the presence of uncertain and variable parameters. The studied UAV is an over-actuated system due the number of actuator control inputs. It can modify the length and the angles between its four arms in different ways, which result an important variation in its Center of Gravity (CoG), inertia, and control matrix. The proposed FTSMC offers many advantages such as, reaching the desired states in a finite-time unlike the conventional sliding mode, robustness vis-a-vis uncertain and unknown parameters, fast convergence towards the sliding surface, high accuracy and reducing the chattering phenomena. Furthermore, the closed-loop stability of the this UAV is ensured by the Lyapunov theory. The eight actuators used to rotate and extend the UAV arms are controlled by simple Proportional Integral Derivative (PID) controllers. Lastly, the robustness and efficiency of the proposed controller are evaluated through a flight scenario, where the UAV geometric parameters are variable over time.

**Keywords:** reconfigurable UAV; variable structure; over-actuated system; Fast Terminal Sliding Mode Controller (FTSMC); Fast Sliding Surface (FSS); uncertain and unknown parameters; PID controller



**Citation:** Derrouaoui, S.H.; Bouzid, Y.; Guiatni, M. Nonlinear Robust Control of a New Reconfigurable Unmanned Aerial Vehicle. *Robotics* **2021**, *10*, 76. <https://doi.org/10.3390/robotics10020076>

Academic Editor: Lorenzo Pollini

Received: 1 April 2021  
Accepted: 21 May 2021  
Published: 23 May 2021

**Publisher's Note:** MDPI stays neutral with regard to jurisdictional claims in published maps and institutional affiliations.



**Copyright:** © 2021 by the authors. Licensee MDPI, Basel, Switzerland. This article is an open access article distributed under the terms and conditions of the Creative Commons Attribution (CC BY) license (<https://creativecommons.org/licenses/by/4.0/>).

## 1. Introduction

### 1.1. Definition

Aerial reconfiguration, is a structural variation of the Unmanned Aerial Vehicle (UAV) in flight to achieve certain particular tasks or missions by adapting its shape or to minimize the consumed energy by seeking the optimal configuration. This aerial operation can be done in the hover phase or in the full flight phase with a slow or fast speed, where it is performed by a new generation of UAVs called: reconfigurable UAVs.

### 1.2. Related Works

During these last years, reconfigurable UAVs have occupied a prominent place in the domain of flying systems and robotics. These new drones can eliminate several problems encountered in the conventional UAVs such as, the flying in congested areas, building inspection, fixed mechanical structure, design complexity, energy consumption, fault tolerant control and obstacles avoidance [1–5]. They are a promising solution in the near future due to their shape characteristics. They allow increasing considerably the capabilities and performance of classical drones in terms of multi-functionalities using variable structure, geometric adaptation, surfaces inspection, energy consumption by exploiting the change of their morphology, maneuverability, obstacles avoidance and fault tolerant control using their high agility [5–7].

Brown et al. [8], have developed a reconfigurable aerial vehicle with foldable arms for inspecting the works of the mines from one borehole. The small size of the designed drone allows it to achieve this objective and to transport a suitable payload for autonomous missions. However, the real reconfiguration process in flight was not tested in this work. More recently, Papadimitriou et al. [9], have proposed a new quadrotor with variable arms.

The variation of these latter depends on the flight environment and the assigned tasks. However, the authors have only considered two flight configurations ( $X, H$ ), which make the proposed quadrotor limited to achieve other flight scenarios and missions such as, inspection of vertical surfaces and crossing of horizontal openings. A Linear Quadratic Regulator (LQR) has been proposed by Wallace et al. [10], to control a small morphing quadrotor in flight. While the obtained results are not satisfactory in terms of stability due to the mechanical design complexity. Recently, Bucki et al. [11], have controlled the attitude of a small UAV with a variable mechanical structure using a LQR. The same control strategy has been adopted by Bai et al. [12], to control a transformable UAV. Nevertheless, the various flight tests have shown that, the proposed controller has not been guaranteed the stability along the pitch and roll axes. Moreover, it has not proven its effectiveness in asymmetric configurations. Meiri et al. [13], have presented a new design of a reconfigurable hybrid UAV. This robot can reduce its size by folding its arms vertically to fly in crowded spaces. The control problem of this type of UAVs has not been treated in this paper. Desbiez et al. [14], have studied the design of a quadcopter with two rotating independent arms. The attitude of the studied UAV has been controlled using standard PID. The same controller has been used to control and stabilize reconfigurable quadrotors with extendable arms in the series of references [15–17]. To optimize the consumed energy and in order to choose the appropriate configuration for each flight phase, a LQR has been applied to control a reconfigurable UAV for different flight scenarios [18,19]. A conventional PID controller has been exploited by Riviere et al. [20], in order to stabilize a quadrotor with variable mechanical structure. However, the stability along the  $x$ -axis has not been ensured. Rizon et al. [21] have presented an adaptive structure of an UAV with changeable arm lengths, to improve the design of classical UAVs. However, the developed model does not consider the changes of the geometric parameters. Hedayati et al. [22], have focused their study on a new particular design of an aerial robot, which based mainly on an expandable scissor structure in order to avoid crashes with humans and obstacles. The control loop has not been study in this work. Shi et al. in work [23], have used a Linear Quadratic Integral (LQI) to control a reconfigurable multilink UAV. The applied controller has not proven its efficiency in terms of stability.

The detailed synthesis of the various research works allows us to conclude that, the authors invested in the control strategies either in the UAVs with extendable arms or with rotating arms contrary to our UAV, which combines the two models. Moreover, due the novelty of these drones and the complexity of their control strategy, they have not applied robust and non linear controllers. Besides, the linear control strategies proposed by the various researchers are not very suitable for reconfigurable UAVs.

Following our previous researches [24], the principal contribution of this work is to propose a nonlinear robust Fast Terminal Sliding Mode controller (FTSMC), to guarantee the flight stability and rapid convergence of the variables states in finite-time of a new reconfigurable UAV. In addition, the robustness of the FTSMC will be tested against uncertain parameters of the variable drone geometry. Notice that, the control architecture of this generation of UAVs is differently to the conventional ones, which makes it a very difficult task. Moreover, the proposed controller has not been applied to these new UAVs in the existing literature sources.

### 1.3. Structure of the Paper

This manuscript is organized as follows:

In Section 2, we present the design and modeling of our reconfigurable UAV. The details of the Fast Terminal Sliding Mode controller (FTSMC) design are presented in Section 3. Simulations and interpretation are displayed in Section 4. Section 5, is devoted to the conclusion and future works.

## 2. Drone Design and Modeling

In this Section, we will briefly describe the design and generic modeling of the proposed UAV. The mathematical development and design steps are detailed in references [24,25].

### 2.1. Drone Design

The reconfigurable UAV combines the designs and advantages of two other transformable drones as shown in Figures 1 and 2. We can exploit it as: a foldable drone where it can change only the angles  $\alpha_i(t)|_{i=1,\dots,4}$  between its arms or as a morphing drone where it can change only the arm lengths  $d_i(t)|_{i=1,\dots,4}$  and in the third case we can use the two types at the same time (rotation and extension).

From the principal configuration, we can have many other configurations by rotating or extending the arms of the drone. Furthermore, by modifying the angular speeds of the rotors  $\Omega_i|_{i=1,\dots,4}$  or the rotation of the arms (primary and secondary) or the length arms, the drone can produce different movements as roll, pitch, yaw and translation. These movements are carried out by actuating the rotation servomotors or translation mechanisms, which make the drone an over actuated system with twelve inputs (see Figure 1).

The composition of the designed drone is shown in Figure 1.

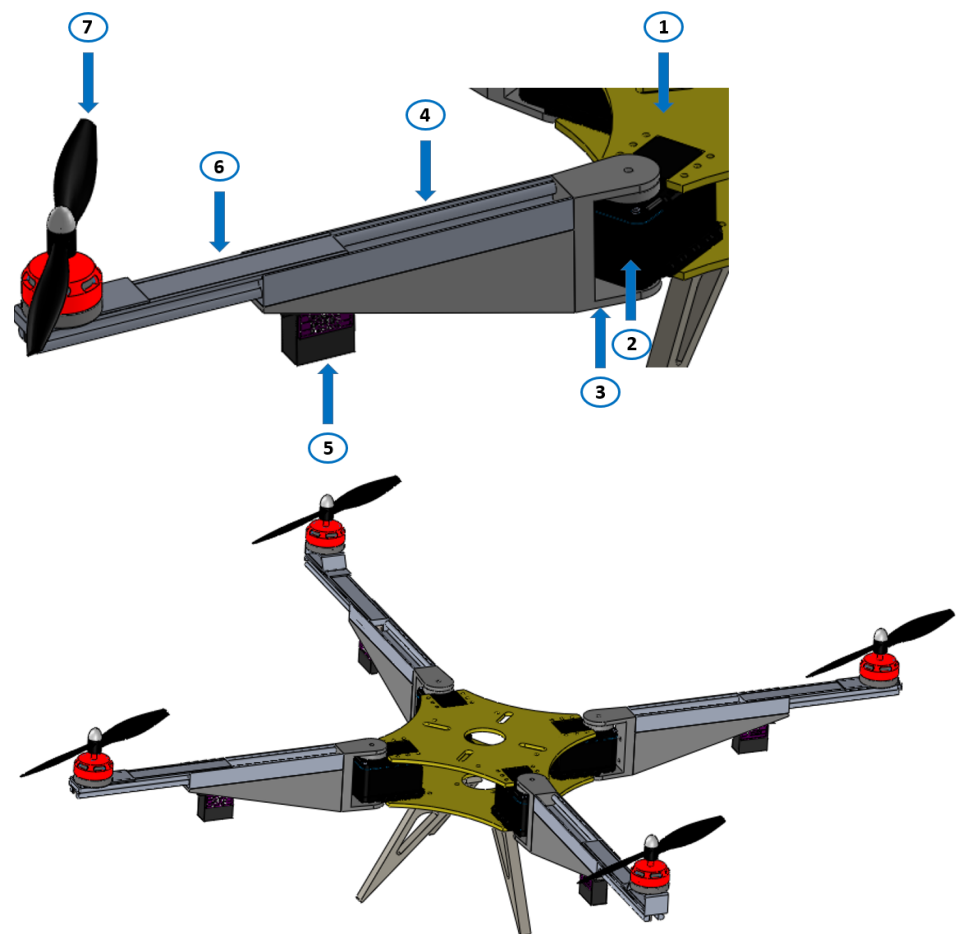


**Figure 1.** UAV composition: (1) Main body, (2) Servomotor AX-12 used for the rotation of the arm, (3) Servo-arm junction, (4) Primary arm, (5) Servomotor used for the extension of the arm, (6) Secondary arm, (7) Propeller.

Note that we have used in the design light and very simple servomotors for the extension of arms. For the rotation of the arms, we have exploited fast servomotors in order to increase the rapidity of the aerial reconfiguration operation.

The different dimensions and parameters of the designed structure are deduced from the Computer Assisted Design (CAD) under the SolidWorks software [24].

We have limited our choice in this work on five different morphologies as shown in Table 1.

**Table 1.** UAV morphologies.

Morphology	Arm Angles and Lengths
x	$\alpha_1(t) = \pi/4, \alpha_2(t) = \pi/4, \alpha_3(t) = \pi/4, \alpha_4(t) = \pi/4$ $d_1(t) = 0, d_2(t) = 0, d_3(t) = 0, d_4(t) = 0$
Y	$\alpha_1(t) = \pi/4, \alpha_2(t) = \pi/4, \alpha_3(t) = \pi/2, \alpha_4(t) = 0$ $d_1(t) = L, d_2(t) = L, d_3(t) = L, d_4(t) = L$
T	$\alpha_1(t) = 0, \alpha_2(t) = \pi/2, \alpha_3(t) = \pi/2, \alpha_4(t) = 0$ $d_1(t) = L, d_2(t) = L, d_3(t) = L, d_4(t) = L$
YI	$\alpha_1(t) = \pi/2, \alpha_2(t) = 0, \alpha_3(t) = \pi/4, \alpha_4(t) = \pi/4$ $d_1(t) = L, d_2(t) = L, d_3(t) = L, d_4(t) = L$
H	$\alpha_1(t) = \pi/2, \alpha_2(t) = 0, \alpha_3(t) = \pi/2, \alpha_4(t) = 0$ $d_1(t) = 0, d_2(t) = 0, d_3(t) = 0, d_4(t) = 0$

These morphologies are described as: small “x” configuration, is used to cross horizontal and vertical spaces, to navigate in more crowded places and to optimize the consumed energy by reducing the dimensions of its structure. “Y” configuration, allows the UAV to move forward without changing the speed of the rear motors. “YI” configuration, allows the UAV to back off without changing the speeds of the front motors. Consequently, these last two configurations lead to an increase in maneuverability around the “ $y_m$ ”-axis and a decrease around the “ $x_m$ ”-axis. “T” configuration is suitable to check and inspect vertical infrastructures. Small “H” configuration, which allows to navigate in horizontally narrow places and to transport and to grab objects.

**Assumption 1.** *The switching operation between the configurations is done in the hover phase with a slow speed.*

## 2.2. Drone Modeling

Recently, few researchers have been interested in the modeling of reconfigurable UAVs. This is explained simply by the complexity and variable dynamic of their model compared to the standards UAVs. Some researchers have supposed that the drone is symmetrical in order to facilitate its study, which means the CoG, inertia and control matrix are constant [10,15–17,21,26]. Others have proposed platform prototypes where the arms are not independent in rotation and extension [12,14,27,28]. Differently to these works, we have developed a new generic model that represents our reconfigurable UAV, where all the variations of the UAV configuration are taken into account [24].

The global position of the CoG changes when the configuration varies. Consequently, the inertia matrix  $\mathcal{I}_{3 \times 3}(\alpha_i(t), d_i(t))$ , roll  $\tau_\varphi(\alpha_i(t), d_i(t))$  and pitch  $\tau_\theta(\alpha_i(t), d_i(t))$  moments in this case vary depending on the arm angles  $\alpha_i(t)$  and the arm extensions  $0 \leq d_i(t) \leq L$  as shown in Figure 2.

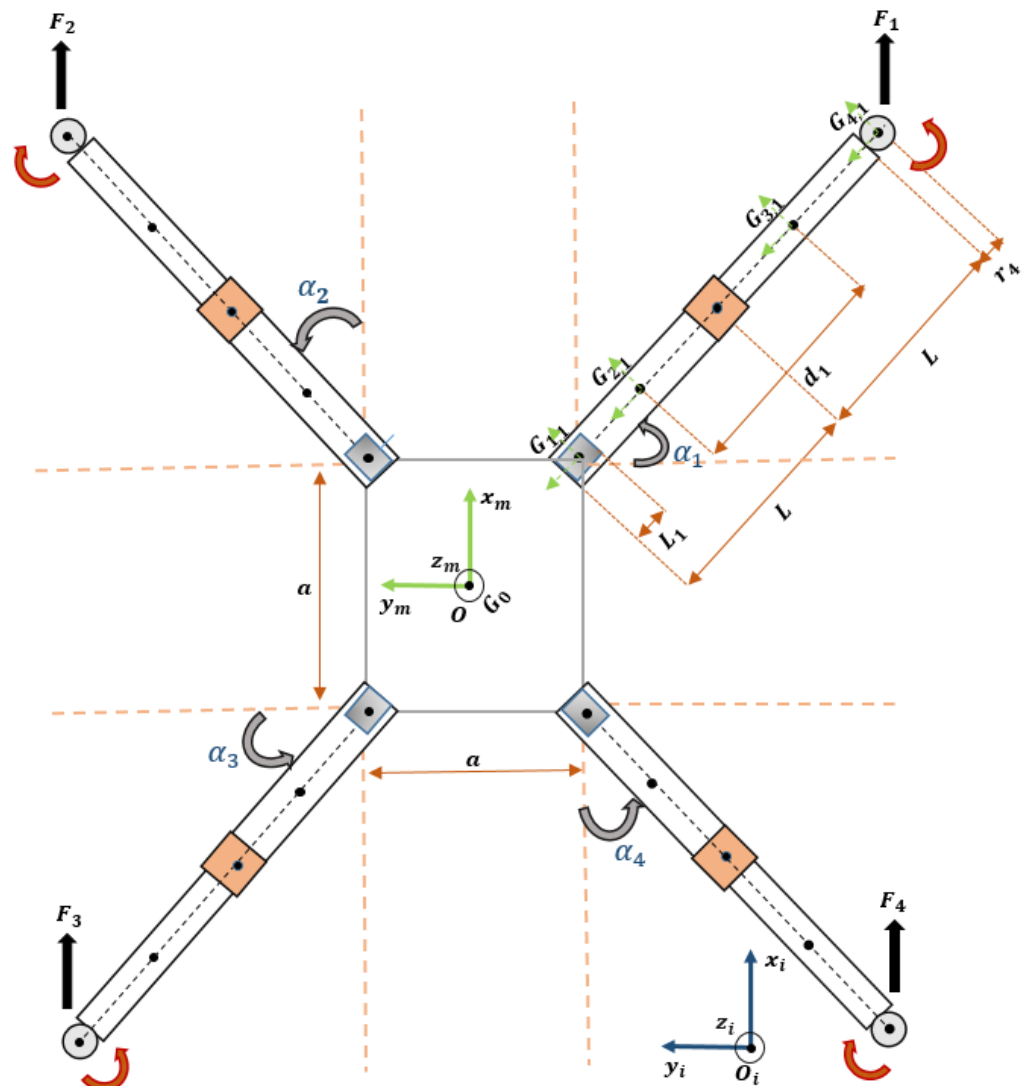


Figure 2. Reconfigurable UAV schematic.

The linear and the angular velocity vectors of the body in the mobile frame  $\mathfrak{R}_m$ , are represented respectively:  $\Lambda^m = (u, v, w)^T \in \mathbb{R}^3$  and  $\zeta = (p, q, r) \in \mathbb{R}^3$ .

Let  $Y = (\varphi, \theta, \psi)^T \in \mathbb{R}^3$  describes the orientation of the mobile and  $\xi = (x, y, z)^T \in \mathbb{R}^3$  denotes its position in the fixed frame  $\mathfrak{R}_i$ .

The relation between the velocities and the external forces  $f^m = (f_x^m, f_y^m, f_z^m)^T \in \mathbb{R}^3$  and moments  $\phi^m = (\phi_x^m, \phi_y^m, \phi_z^m)^T \in \mathbb{R}^3$  applied to CoG, can be presented using Newton-Euler formalism as:

$$\begin{bmatrix} m\mathcal{J}_{3 \times 3}(\alpha_i(t), d_i(t)) & O_{3 \times 3} \\ O_{3 \times 3} & \mathcal{J}_{3 \times 3}(\alpha_i(t), d_i(t)) \end{bmatrix} \begin{bmatrix} \dot{\Lambda}^m \\ \dot{\zeta} \end{bmatrix} + \begin{bmatrix} \zeta \times m\Lambda^m \\ \zeta \times \mathcal{J}(\alpha_i(t), d_i(t))\zeta \end{bmatrix} = \begin{bmatrix} f^m \\ \phi^m \end{bmatrix} \quad (1)$$

### 2.3. Control Matrix

The control matrix  $\Delta(\alpha_i(t), d_i(t)) \in \mathbb{R}^{4 \times 4}$  transforms the angular speeds of the propellers  $\Omega_i^2|_{i=1, \dots, 4}$  to a total thrust force  $\mathcal{T}$  and moments  $\tau_\varphi, \tau_\theta, \tau_\psi$ . It can be represented as follows:

$$\Delta = \begin{bmatrix} b & b[y_{4,1}(t) - y_G(t)] & b[x_G(t) - x_{4,1}(t)] & d \\ b & b[y_{4,2}(t) - y_G(t)] & b[x_G(t) - x_{4,2}(t)] & -d \\ b & b[y_{4,3}(t) - y_G(t)] & b[x_G(t) - x_{4,3}(t)] & d \\ b & b[y_{4,4}(t) - y_G(t)] & b[x_G(t) - x_{4,4}(t)] & -d \end{bmatrix}^T \quad (2)$$

where  $b$  and  $d$  are the thrust and drag coefficients, respectively and  $(x_{4,i}, y_{4,i})$  are the CoG coordinates of the rotors.

The proposed UAV has twelve control inputs, where  $u_1 = \mathcal{T}, u_2 = \tau_\varphi, u_3 = \tau_\theta, u_4 = \tau_\psi$  are used for the control of its altitude and attitude, while  $u_5, u_6, u_7, u_8$  to control the arms rotation and  $u_9, u_{10}, u_{11}, u_{12}$  to control the arms extension.

### 3. Drone Control

#### 3.1. Control Architecture

The reconfigurable drone is characterized by its variable parameters according to the change of its structure. Furthermore, the proposed Fast Terminal Sliding Mode Control (FTSMC) will be applied and tested in the presence of these uncertain parameters, such as CoG, inertia, arm angles  $\alpha_i(t)$ , arm lengths  $d_i(t)$  and control matrix, in order to ensure that the state variables converge rapidly towards the Fast Sliding Surface (FSS) and consequently to the equilibrium point in finite-time.

The rotation of the servomotors attached to the main body causes a variation of the arms (primary and secondary) by angles  $\alpha_i$ , while the rotation of the servomotors attached to the primary arms by angles  $\gamma_i$  generates an extension of the secondary arms by distances  $d_i$ . These variations ( $\alpha_i$  and  $d_i$ ) are sent to the different blocks to calculate the control matrix, inertia as well as the CoG (see Figure 3).

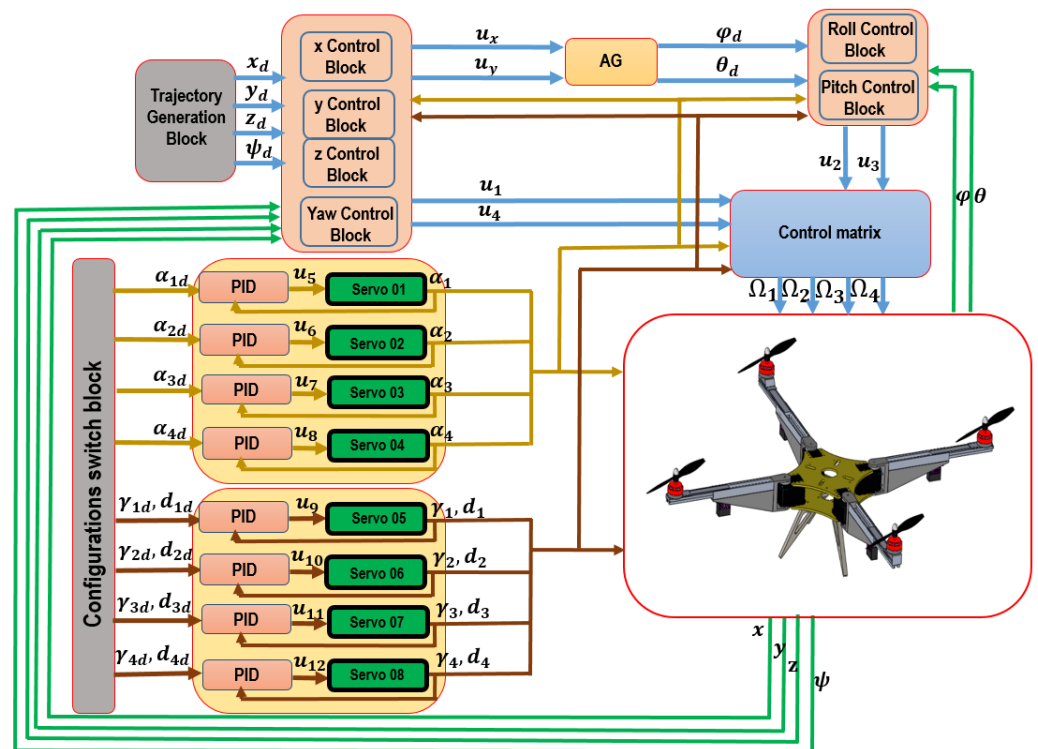


Figure 3. Control architecture.

The desired trajectories are generated by a trajectory generator block as shown in Figure 3. The attitude and translations of our UAV are controlled in two ways, either varying the position of the arms, or by the angular speeds of the four rotors.

The two controls  $u_x$  and  $u_y$  are used to calculate the desired roll and pitch angles.

The servomotors used to rotate and extend the arms are controlled by conventional PID controllers (see Figure 3) as:

$$u_j = K_{Pj}e_j + K_{Ij} \int_0^t e_j dt + K_{Dj}\dot{e}_j \tag{3}$$

with  $e_j$  is the tracking error.  $K_{Pj}$ ,  $K_{Ij}$  and  $K_{Dj}$  are constant gains.  $j = 5, \dots, 12$ .

The model used to design the controller is given by Equation (4) as:

$$\begin{cases} \ddot{\varphi} &= \beta_1(t)\dot{\theta}\dot{\psi} + \beta_2(t)\dot{\theta}\Omega_r + \beta_3(t)u_2 + \beta_4(t)\dot{\varphi}^2 \\ \ddot{\theta} &= \beta_5(t)\dot{\varphi}\dot{\psi} + \beta_6(t)\dot{\varphi}\Omega_r + \beta_7(t)u_3 + \beta_8(t)\dot{\theta}^2 \\ \ddot{\psi} &= \beta_9(t)\dot{\theta}\dot{\varphi} + \beta_{10}(t)u_4 + \beta_{11}(t)\dot{\psi}^2 \\ \ddot{x} &= u_1 \frac{u_x}{m} + \beta_{13}\dot{x} \\ \ddot{y} &= u_1 \frac{u_y}{m} + \beta_{14}\dot{y} \\ \ddot{z} &= -g + u_1 \frac{c_\varphi c_\theta}{m} + \beta_{12}\dot{z} \end{cases} \tag{4}$$

where

$$\begin{aligned} u_x &= c_\psi s_\theta c_\varphi + s_\psi s_\varphi, u_y = s_\psi s_\theta c_\varphi - c_\psi s_\varphi \\ \beta_1(t) &= \frac{I_{yy}(\alpha_i(t), d_i(t)) - I_{zz}(\alpha_i(t), d_i(t))}{I_{xx}(\alpha_i(t), d_i(t))}, \beta_2(t) = \frac{-\mathfrak{J}_r}{I_{xx}(\alpha_i(t), d_i(t))}, \beta_3(t) = \frac{1}{I_{xx}(\alpha_i(t), d_i(t))} \\ \beta_4(t) &= \frac{-\mathcal{K}_{Ax}}{I_{xx}(\alpha_i(t), d_i(t))}, \beta_5(t) = \frac{I_{zz}(\alpha_i(t), d_i(t)) - I_{xx}(\alpha_i(t), d_i(t))}{I_{yy}(\alpha_i(t), d_i(t))}, \beta_6(t) = \frac{\mathfrak{J}_r}{I_{yy}(\alpha_i(t), d_i(t))} \\ \beta_7(t) &= \frac{1}{I_{yy}(\alpha_i(t), d_i(t))}, \beta_8(t) = \frac{-\mathcal{K}_{Ay}}{I_{yy}(\alpha_i(t), d_i(t))}, \beta_9(t) = \frac{I_{xx}(\alpha_i(t), d_i(t)) - I_{yy}(\alpha_i(t), d_i(t))}{I_{zz}(\alpha_i(t), d_i(t))} \\ \beta_{10}(t) &= \frac{1}{I_{zz}(\alpha_i(t), d_i(t))}, \beta_{11}(t) = \frac{-\mathcal{K}_{Az}}{I_{zz}(\alpha_i(t), d_i(t))}, \beta_{12} = \frac{-\mathcal{K}_{Dz}}{m}, \beta_{13} = \frac{-\mathcal{K}_{Dx}}{m}, \beta_{14} = \frac{-\mathcal{K}_{Dy}}{m}, \\ \Omega_r &= \sum_{i=1}^4 (-1)^{i+1} \Omega_i^2 \end{aligned}$$

### 3.2. Fast Terminal Sliding Mode Control (FTSMC) Design

This subsection details the design of the robust nonlinear controller for a new reconfigurable UAV to test its robustness in the presence of uncertain and variable parameters. These latter are directly related to the desired configuration during the flight.

**Lemma 1.** *Considering the Fast Sliding Surface (FSS) as:*

$S = \dot{e} + \mathfrak{N}e + \mathfrak{T}e^{\frac{\alpha}{\beta}}$ , with  $\mathfrak{N} > 0$ ,  $\mathfrak{T} > 0$ , and  $\alpha, \beta$  are positive odd integers satisfying  $\alpha < \beta$ . The time  $t_s$  to reach quickly  $e(t_s) = 0$  is defined as:

$$t_s = \frac{1}{\mathfrak{N}(1 - \frac{\alpha}{\beta})} \ln \frac{\mathfrak{N}|e(t_0)|^{(1 - \frac{\alpha}{\beta})} + \mathfrak{T}}{\mathfrak{T}}$$

**Proof.** To demonstrate the formula of  $t_s$ , we assume that the variable states reach their desired states, which means:

$$S = \dot{S} = 0 \tag{5}$$

In this case, we have:

$$\dot{e} = -\mathfrak{N}e - \mathfrak{T}e^{\frac{\alpha}{\beta}} \tag{6}$$

We integrate Equation (6) as:

$$\int_{e(t_0)}^{e(t_s)} \frac{de}{-\mathfrak{N}e - \mathfrak{T}e^{\frac{\alpha}{\beta}}} = \int_{t_0}^{t_s} dt \tag{7}$$

Lastly, the formulas of  $t_s$  is obtained as follows:

$$t_s = \frac{1}{\mathfrak{N}(1 - \frac{\alpha}{\beta})} \ln \frac{\mathfrak{N}|e(t_0)|^{(1 - \frac{\alpha}{\beta})} + \mathfrak{T}}{\mathfrak{T}} \tag{8}$$

□

The Fast Terminal Sliding Mode Control of the first subsystem of (4) is designed as:

$$u_2 = \frac{1}{-\beta_3(t)} [(\mathfrak{N}_\varphi + \mathfrak{T}_\varphi \frac{\alpha_\varphi}{\beta_\varphi} e_\varphi^{(\frac{\alpha_\varphi - \beta_\varphi}{\beta_\varphi})}) \dot{e}_\varphi + \eta_\varphi S_\varphi + \sigma_\varphi S_\varphi^{\frac{\alpha_\varphi}{\beta_\varphi}} + \beta_1(t) \dot{\theta} \dot{\psi} + \beta_2(t) \dot{\theta} \Omega_r + \beta_4(t) \dot{\varphi}^2 - \dot{\varphi}_d] \tag{9}$$

with  $\eta, \sigma$  are positive parameters.

**Theorem 1.** *Considering the first subsystem of (4), with the designed controller (9), then the state variable  $\varphi$  of the first subsystem (4) converges to the FSS  $S_\varphi$  in a finite time. Furthermore, the asymptotic stability is assured using the Lyapunov function.*

**Proof.** Let us choose  $e_\varphi$ , as a tracking error of the first subsystem:

$$e_\varphi = \varphi - \varphi_d \tag{10}$$

The dynamics of (10) is given as:

$$\dot{e}_\varphi = \dot{\varphi} - \dot{\varphi}_d \tag{11}$$

When the variable state  $\varphi$  is far from the desired state  $\varphi_d$ , which means  $e_\varphi \neq 0$ , and to accelerate its convergence to the equilibrium point, the Fast Terminal Sliding Mode Surface is constructed as [29,30]:

$$S_\varphi = \dot{e}_\varphi + \mathfrak{N}_\varphi e_\varphi + \mathfrak{T}_\varphi e_\varphi^{(\frac{\alpha_\varphi}{\beta_\varphi})} \tag{12}$$

The derivative of  $S_\varphi$  is expressed as follows:

$$\dot{S}_\varphi = \ddot{e}_\varphi + \mathfrak{N}_\varphi \dot{e}_\varphi + \mathfrak{T}_\varphi \frac{\alpha_\varphi}{\beta_\varphi} e_\varphi^{(\frac{\alpha_\varphi - \beta_\varphi}{\beta_\varphi})} \dot{e}_\varphi \tag{13}$$

The Lyapunov function candidate is given by:

$$V_\varphi = \frac{1}{2} S_\varphi^2 \tag{14}$$

Differentiating  $V_\varphi$  with respect to time, we get:

$$\dot{V}_\varphi = S_\varphi \dot{S}_\varphi \tag{15}$$

Substitute Equations (9) and (13) in Equation (15), we have:

$$\dot{V}_\varphi = -\eta_\varphi |S_\varphi|^2 - \sigma_\varphi S_\varphi^{(\frac{\alpha_\varphi + \beta_\varphi}{\beta_\varphi})} < 0 \tag{16}$$

From Equation (16), it is obvious that the variable states converge towards their desired states in finite time, as well as the FSS converges to zero. Moreover, the asymptotic stability is guaranteed.  $\square$

To prove the asymptotic stability and extract the other controllers, we follow the same steps above.

### 3.3. Optimization

In order to select the best FTSMC parameters, we will use a metaheuristic algorithm based on Particle Swarm Optimization (PSO) [31]. This algorithm is based mainly on swarm particles  $N$ , where each particle  $i$  can be a solution for the treated problem. In the initialization step, the positions and velocities of the particles are generated randomly. Then, fitness function of each particle is evaluated and tested to update after the local best  $p_{best}$  as well as the global best  $g_{best}$ , which correspond to the smallest fitness value in the

swarm. In the last step of the algorithm, the particle's position and velocity are calculated and updated according to Equations (17) and (18) respectively.

$$V_{ij}(t+1) = wV_{ij}(t) + R_1C_1(p_{bestij} - X_{ij}(t)) + R_2C_2(g_{bestij} - X_{ij}(t)) \quad (17)$$

$$X_{ij}(t+1) = X_{ij}(t) + V_{ij}(t+1) \quad (18)$$

where

$i = 1, 2, \dots, N$ .

$j = 1, 2, \dots, D$ .

$D$  is the dimension of the search space.

$w$  is the inertia coefficient.

$C_1, C_2$  are the learning factors.

$R_1, R_2$  are random variables generated from a uniform distribution in  $[0,1]$ .

$V_{ij}$  is the particle velocity.

$X_{ij}$  is the particle position.

The optimal gains of the FTSMC using PSO algorithm are summarized in Table 2.

**Table 2.** Optimal parameters of the FTSMC.

Parameter	Value
$\alpha_{\varphi,\theta,\psi,z}$	11
$\beta_{\varphi,\theta,\psi,z}$	13
$\mathfrak{N}_{\varphi,\theta,\psi,z}$	9.77
$\mathfrak{T}_{\varphi,\theta,\psi,z}$	6.83
$\eta_{\varphi,\theta,\psi,z}$	0.41
$\sigma_{\varphi,\theta,\psi,z}$	1.18

#### 4. Simulation Results

In this scenario, the accuracy, fast convergence, decreasing the chattering, stability and robustness of the proposed FTSMC are evaluated taking into account the uncertainty and variation of UAV parameters.

##### 4.1. Flight Scenario

The reconfigurable UAV must fly at a fixed altitude of 10 m and passes through five waypoints of coordinates  $(0,0,0)$ ,  $(0,0,10)$ ,  $(4,0,10)$ ,  $(4,4,10)$ ,  $(0,4,10)$  as shown in Figure 6. At the points  $(0,0,10)$ ,  $(4,0,10)$ ,  $(4,4,10)$ ,  $(0,4,10)$ , we consider that the UAV stops to take several photos, and changes its morphology in order to take the most suitable configuration to the path to reach the next point. From the starting point  $(0,0,0)$ , the UAV begins to rise vertically with the small "x" configuration to achieve the point  $(0,0,10)$ . After 10 s, it stabilizes at this point, it changes its aerial morphology to "Y", and then it takes photos during 10 seconds. After, it starts to move to the point  $(4,0,10)$ . At this point, it changes its configuration to the "T" configuration in order to check and inspect the vertical infrastructures and to reach the next point  $(4,4,10)$ , and it stops for 10 s to take photos. Once at the point  $(4,4,10)$ , it changes its morphology to "YI" to reach the point  $(0,4,10)$  and it pauses for 10 seconds to take photos. Afterwards, at the point  $(0,4,10)$  it changes to the last "H" configuration, in order to pass laterally through a horizontally narrow space to achieve the point  $(0,0,10)$  and it stops at the altitude of 10 m, with the same previous duration to take photos.

Note that, we have experimented with other sets of parameters before the optimization step, but these parameters occur some instability and system performance degradation in terms of steady state error, response time, and overshoot especially for the complex configurations (H,Y,YI,T).

The optimal parameters considered in simulation for the FTSMC are listed in Table 2. To achieve the best PID parameters, simulations are performed for different position goals using the closed loop model of servomotors AX-12, where the  $k_p$ ,  $k_I$  and  $k_D$  parameters are tuned manually to reach a similar response in terms of steady state error, response time, and overshoot with the real servomotor response. The obtained PID gains are shown in Table 3.

**Table 3.** PID servo-controller gains.

Gains	$K_{Pj}$	$K_{Ij}$	$K_{Dj}$
Value	18.23	8.09	0.54

4.2. Simulations

Simulation results are illustrated in Figures 4–11.

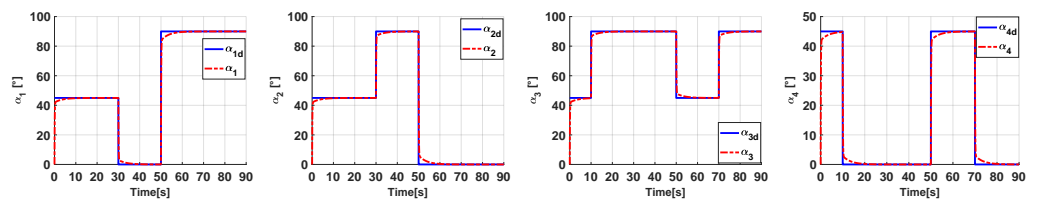


**Figure 4.** Evolution of servomotor angles.

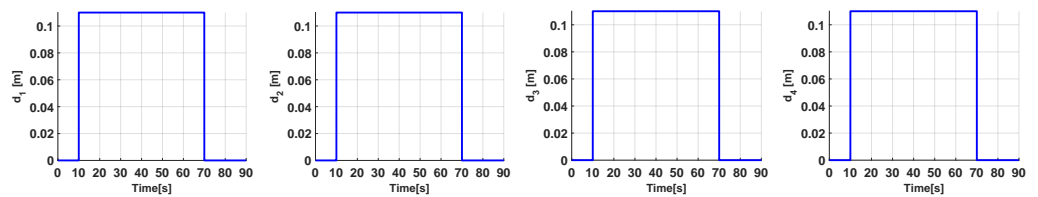


**Figure 5.** Evolution of arm lengths.

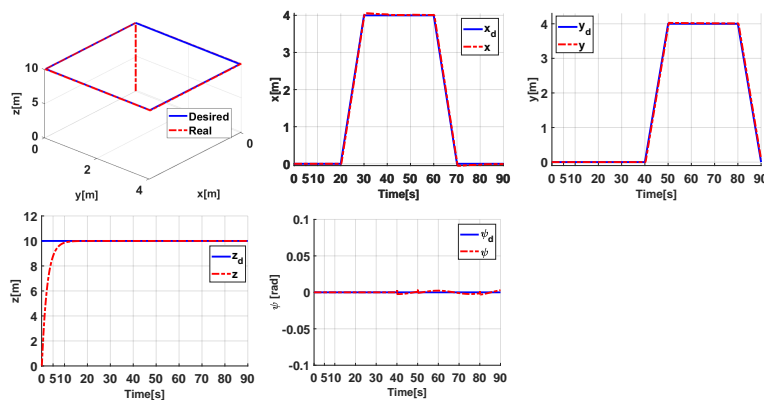


**Figure 6.** 3D trajectory and  $\psi$  angle of the FTSMC.

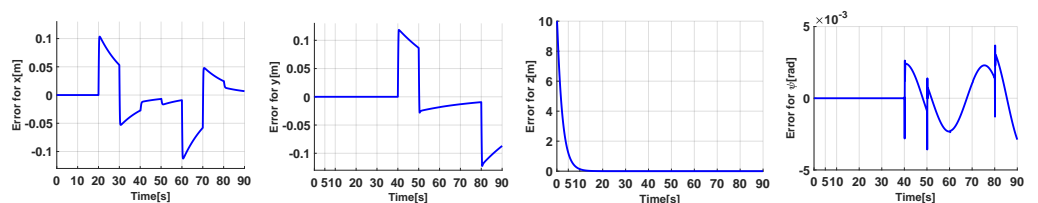


**Figure 7.** Errors of the FTSMC.

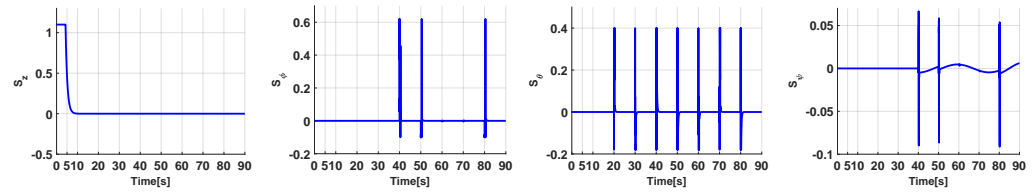


Figure 8. Sliding surfaces of the FTSMC.

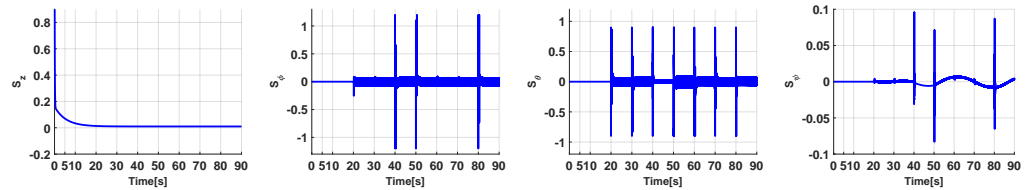


Figure 9. Sliding surfaces of the SMC.

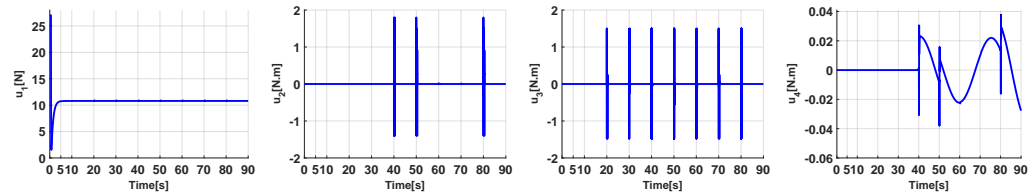


Figure 10. Control signals of the FTSMC.

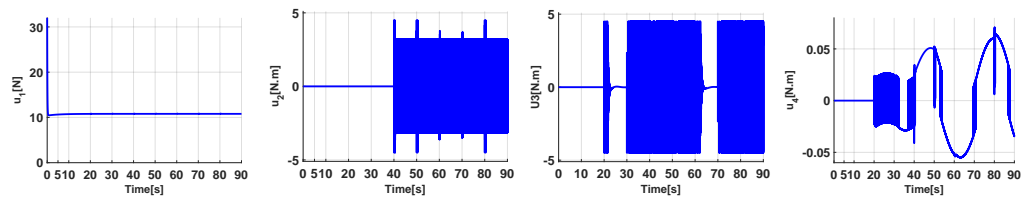


Figure 11. Control signals of the SMC.

### 4.3. Results Interpretation

Figure 4 represents the evolution of the output positions of the servomotors used to rotate the four arms of the UAV. In addition, the reconfigurable UAV changes the position of its servomotors and therefore its arms, to obtain the different flight configurations  $(x, Y, T, YI, H)$ . It is observed that the outputs of the four servomotors  $(\alpha_1, \alpha_2, \alpha_3, \alpha_4)$  achieve their desired positions  $(\alpha_{1d}, \alpha_{2d}, \alpha_{3d}, \alpha_{4d})$  at about 5 s. The errors observed in the descent and ascent are generated due to the variation of the arms positions. Once the desired positions are reached, the errors converge towards zero. Moreover, Figure 5 shows the variation of the arms extension  $d_i(t)$  of the considered configurations  $(x, Y, T, YI, H)$  over time.

It is observed in Figures 6 and 7, the quick convergence of the variable states  $(x, y, z, \psi)$  to their desired states  $(x_d, y_d, z_d, \psi_d)$  in finite-time. In addition, Figure 7, shows that the FTSMC is able to track the desired path with high accurate.

The control signal  $u_1$  shown in Figure 10, which corresponds to the altitude  $z$  and the sliding surface  $S_z$ , is at its maximum in the start before to stabilize around a constant value (11N).

The change of the two control signals  $u_2$  and  $u_3$  are due to the change of configuration during flight and the trajectories  $y_d$  and  $x_d$ . They also depend on the dynamic of  $S_\varphi$  and  $S_\theta$  (see Figures 6, 8 and 10).

For the yaw angle  $\psi$ , there is a very slight deviation in the system response as displayed in Figures 6. This is illustrated by the cancellation of the error in Figure 7 and by the very low values of  $u_4$  and  $S_\psi$  (see Figures 8 and 10).

The sliding surfaces  $(S_\varphi, S_\theta, S_\psi, S_z)$  displayed in Figure 8, converge rapidly to zero in finite time. We can interpret this rapidity by adding the term  $\mathfrak{T}e^{\frac{\alpha}{\beta}}$  in the sliding surface.

Clearly, the FTSMC has decreased the chattering phenomena and the energy consumption unlike the conventional Sliding Mode (SM) (see Figures 8–11), and this is explained by the absence of the “*sign*” function. Moreover, the FTSMC has guaranteed the flight stability and the fast convergence of the states towards the equilibrium point and it was robust in the face of the change of the aerial morphology of our reconfigurable UAV.

## 5. Conclusions and Future Works

In this work, the design of a new reconfigurable UAV was presented briefly. The dynamic model is developed based on the mechanical laws (Newton–Euler). In order to achieve the desired states in finite time and to ensure flight stability, a FTSMC was designed and applied. Moreover, the fast convergence to the sliding surface and the robustness have been tested against uncertain system parameters. From the simulation results we can conclude that, the controller has achieved its objectives. Overall, the proposed FTSMC is a promising solution for the control of reconfigurable UAVs, since it allows increasing the capabilities of the classical controllers.

In future works we aim to apply hybrid adaptive robust controllers and make a comparative study with the obtained results of FTSMC. We also wish to experimentally evaluate the influence of environment on the flight of our UAV.

**Author Contributions:** Methodology, Y.B.; software, S.H.D., M.G.; validation, S.H.D., Y.B., M.G.; formal analysis, S.H.D., Y.B., M.G.; writing—original draft preparation, S.H.D.; writing—review and editing, S.H.D.; visualization, M.G.; funding acquisition, Y.B., M.G. All authors contributed equally to this work. All authors have read and agreed to the published version of the manuscript.

**Funding:** This research received no external funding.

**Conflicts of Interest:** The authors declare no conflict of interest.

## References

- da Ferreira, M.A.; Begazo, M.F.T.; Lopes, G.C.; de Oliveira, A.F.; Colombini, E.L.; da Simões, A. Drone reconfigurable architecture (dra): A multipurpose modular architecture for Unmanned Aerial Vehicles (UAVs). *J. Intell. Robot. Syst.* **2020**, *99*, 517–534. [[CrossRef](#)]
- da Ferreira, M.A.; Lopes, G.C.; Colombini, E.L.; da Simões, A. A novel architecture for multipurpose reconfigurable unmanned aerial vehicle (uav): Concept, design and prototype manufacturing. In Proceedings of the 2018 Latin American Robotic Symposium, 2018 Brazilian Symposium on Robotics (SBR) and 2018 Workshop on Robotics in Education (WRE), João Pessoa, Brazil, 6–10 November 2018; pp. 443–450.
- Junaid, A.B.; da Sanchez, A.D.; Bosch, J.B.; Vitzilaios, N.; Zweiri, Y. Design and implementation of a dualaxis tilting quadcopter. *Robotics* **2018**, *7*, 65. [[CrossRef](#)]
- Barbarino, S.; Bilgen, O.; Ajaj, R.M.; Friswell, M.I.; Inman, D.J. A review of morphing aircraft. *J. Intell. Mater. Syst. Struct.* **2011**, *22*, 823–877. [[CrossRef](#)]
- Derrouaoui, S.H.; Bouzid, Y.; Guiatni, M.; Dib, I. A Comprehensive Review on Reconfigurable Drones: Classification, Characteristics, Design and Control Technologies. *Unmanned Syst.* **2021**, *9*, 1–27.
- Fasel, U.; Keidel, D.; Baumann, L.; Cavolina, G.; Eichenhofer, M.; Ermanni, P. Composite additive manufacturing of morphing aerospace structures. *Manuf. Lett.* **2020**, *23*, 85–88. [[CrossRef](#)]
- Choi, H.C.; Wee, I.; Corah, M.; Sabet, S.; Kim, T.; Touma, T.; Shim, D.H.; Agha-mohammadi, A.-A. Baxter: Bi-modal aerial-terrestrial hybrid vehicle for long-endurance versatile mobility: Preprint version. *arXiv* **2021**, arXiv:2102.02942.
- Brown, L.; Clarke, R.; Akbari, A.; Bhandari, U.; Bernardini, S.; Chhabra, P.; Marjanovic, O.; Richardson, T.; Watson, S. The design of prometheus: A reconfigurable uav for subterranean mine inspection. *Robotics* **2020**, *9*, 95. [[CrossRef](#)]
- Papadimitriou, A.; Mansouri, S.S.; Kanellakis, C.; Nikolakopoulos, G. Geometry aware nmpc scheme for morphing quadrotor navigation in restricted entrances. *arXiv* **2021**, arXiv:2101.02965.
- Wallace, D.A. Dynamics and Control of a Quadrotor with Active Geometric Morphing. Ph.D. Dissertation, Washington University, St. Louis, MO, USA, 2016.
- Bucki, N.; Mueller, M.W. Drone reconfigurable architecture Design and control of a passively morphing quadcopter. In Proceedings of the 2019 International Conference on Robotics and Automation (ICRA), Montreal, QC, Canada, 20–24 May 2019; pp. 9116–9122.
- Bai, Y.; Gururajan, S. Evaluation of a baseline controller for autonomous “figure-8” flights of a morphing geometry quadcopter: Flight performance. *Drones* **2019**, *3*, 70. [[CrossRef](#)]

13. Meiri, N.; Zarrouk, D. Flying star, a hybrid crawling and flying sprawl tuned robot. In Proceedings of the 2019 International Conference on Robotics and Automation (ICRA), Montreal, QC, Canada, 20–24 May 2019; pp. 5302–5308.
14. Desbiez, A.; Expert, F.; Boyron, M.; Dipieri, J.; Viollet, S.; Ruffier, F. X-morf: A crash-separable quadrotor that morphs its x-geometry in flight. In Proceedings of the 2017 Workshop on Research, Education and Development of Unmanned Aerial Systems (RED-UAS), Linköping, Sweden, 3–5 October 2017; pp. 222–227.
15. Kamil, Y.; Hazry, D.; Wan, K.; Razlan, Z.M.; Shahrman, A.B. Design a new model of unmanned aerial vehicle quadrotor using the variation in the length of the arm. In Proceedings of the 2017 International Conference on Artificial Life and Robotics (ICAROB 2017), Miyazaki, Japan, 19–22 January 2017; pp. 723–726.
16. Oktay, T.; Oguz, K. Non simultaneous morphing system design for yaw motion in quadrotors. *J. Aviat.* **2019**, *3*, 81–88.
17. Köse, O.; Oktay, T. Non simultaneous morphing system desing for quadrotors. *Avrupa Bilim Ve Teknol. Derg.* **2019**, *16*, 577–588.
18. Falanga, D.; Kleber, K.; Mintchev, S.; Floreano, D.; Scaramuzza, D. The foldable drone: A morphing quadrotor that can squeeze and fly. *IEEE Robot. Autom. Lett.* **2018**, *4*, 209–216. [[CrossRef](#)]
19. Fabris, A.; Kleber, K.; Falanga, D.; Scaramuzza, D. Geometry aware compensation scheme for morphing drones. In Proceedings of the 2020 IEEE/RSJ International Conference on Intelligent Robots and Systems (IROS), Las Vegas, NV, USA, 25–29 October 2020.
20. Riviere, V.; Manecy, A.; Viollet, S. Agile robotic fliers: A morphing-based approach. *Soft Robot.* **2018**, *5*, 541–553. [[CrossRef](#)] [[PubMed](#)]
21. Rizon, M.; Ang, C.; Solihin, M.I.; Razlan, Z.M.; Desa, H.; Bakar, S.A.; Khairunizam, W.; Ibrahim, Z. Effects of variable arm length on uav control systems. *J. Robot. Netw. Artif. Life* **2020**, *7*, 91–97. [[CrossRef](#)]
22. Hedayati, H.; Suzuki, R.; Leithinger, D.; Szafir, D. Pufferbot: Actuated expandable structures for aerial robots. In Proceedings of the 2020 IEEE/RSJ International Conference on Intelligent Robots and Systems (IROS), Las Vegas, NV, USA, 25–29 October 2020.
23. Shi, F.; Zhao, M.; Murooka, M.; Okada, K.; Inaba, M. Aerial regrasping: Pivoting with transformable multilink aerial robot. In Proceedings of the 2020 IEEE International Conference on Robotics and Automation (ICRA), Paris, France, 31 May–31 August 2020; pp. 200–207.
24. Derrouaoui, S.H.; Guiatni, M.; Bouzid, Y.; Dib, I.; Moudjari, N. Dynamic modeling of a transformable quadrotor. In Proceedings of the International Conference on Unmanned Aircraft Systems (ICUAS), Athens, Greece, 1–4 September 2020; pp. 1714–1719.
25. Derrouaoui, S.H.; Bouzid, Y.; Guiatni, M.; Dib, I.; Moudjari, N. Design and modeling of unconventional quadrotors. In Proceedings of the 2020 28th Mediterranean Conference on Control and Automation (MED), Saint-Raphaël, France, 15–18 September 2020; pp. 721–726.
26. Xiong, H.; Hu, J.; Diao, X. Optimize energy efficiency of quadrotors via arm rotation. *J. Dyn. Syst. Meas. Control* **2019**, *141*, 091002. [[CrossRef](#)]
27. Tuna, T.; Ovrur, S.E.; Gokbel, E.; Kumbasar, T. Folly: A self foldable and self deployable autonomous quadcopter. In Proceedings of the 2018 6th International Conference on Control Engineering and Information Technology (CEIT), Istanbul, Turkey, 25–27 October 2018; pp. 1–6.
28. Pastor, D.; Izraelevitz, J.; Nadan, P.; Bouman, A.; Burdick, J.; Kennedy, B. Design of a ballistically-launched foldable multirotor. In Proceedings of the 2019 IEEE/RSJ International Conference on Intelligent Robots and Systems (IROS), Macau, China, 3–8 November 2019; pp. 5212–5218.
29. Chen, M.; Wu, Q.-X.; Cui, R.-X. Terminal sliding mode tracking control for a class of siso uncertain nonlinear systems. *ISA Trans.* **2013**, *52*, 198–206. [[CrossRef](#)] [[PubMed](#)]
30. Shi, X.; Cheng, Y. Adaptive fast terminal sliding mode (ftsm) control design for quadrotor uav under external windy disturbances. In Proceedings of the 2020 International Conference on Unmanned Aircraft Systems (ICUAS), Athens, Greece, 1–4 September 2020; pp. 512–516.
31. Shi, Y.; Eberhart, R.C. Empirical study of particle swarm optimization. In Proceedings of the IEEE/Proceedings of the 1999 Congress on Evolutionary Computation-CEC99 (Cat. No. 99TH8406), Washington, DC, USA, 6–9 July 1999; Volume 3, pp. 1945–1950.